

## Size-Dependent Catalytic Activity and Dynamics of Gold Nanoparticles at the Single-Molecule Level

Xiaochun Zhou, Weilin Xu, Guokun Liu, Debashis Panda, and Peng Chen\*

*Department of Chemistry and Chemical Biology, Cornell University, Ithaca, New York 14853*

Received May 27, 2009; E-mail: pc252@cornell.edu

**Abstract:** Nanoparticles are important catalysts for petroleum processing, energy conversion, and pollutant removal. As compared to their bulk counterparts, their often superior or new catalytic properties result from their nanometer size, which gives them increased surface-to-volume ratios and chemical potentials. The size of nanoparticles is thus pivotal for their catalytic properties. Here, we use single-molecule fluorescence microscopy to study the size-dependent catalytic activity and dynamics of spherical Au-nanoparticles under ambient solution conditions. By monitoring the catalysis of individual Au-nanoparticles of three different sizes in real time with single-turnover resolution, we observe clear size-dependent activities in both the catalytic product formation reaction and the product dissociation reaction. Within a model of classical thermodynamics, these size-dependent activities of Au-nanoparticles can be accounted for by the changes in the adsorption free energies of the substrate resazurin and the product resorufin because of the nanosize effect. We also observe size-dependent differential selectivity of the Au-nanoparticles between two parallel product dissociation pathways, with larger nanoparticles less selective between the two pathways. The particle size also strongly influences the surface-restructuring-coupled catalytic dynamics; both the catalysis-induced and the spontaneous dynamic surface restructuring occur more readily for smaller Au-nanoparticles due to their higher surface energies. Using a simple thermodynamic model, we analyze the catalysis- and size-dependent dynamic surface restructuring quantitatively; the results provide estimates on the activation energies and time scales of spontaneous dynamic surface restructuring that are fundamental to heterogeneous catalysis in both the nano- and the macro-scale. This study further exemplifies the power of the single-molecule approach in probing the intricate workings of nanoscale catalysts.

### 1. Introduction

Nanoparticles of various materials catalyze many important chemical transformations, including oxidation of hydrocarbons, C–C coupling, hydrogenation–dehydrogenation, and redox.<sup>1–12</sup> As compared to their bulk counterparts, nanoparticles often have superior or even new catalytic properties following from their nanometer size that gives them increased surface-to-volume ratios and chemical potentials. So the size of nanoparticles is pivotal in determining their catalytic properties, and understand-

ing how size affects their catalytic properties remains a central goal in nanocatalysis research.<sup>4,13–26</sup>

Significant work has been done to examine size-dependent catalysis of nanoparticles at the ensemble level.<sup>4,5,13–26</sup> By

- (1) Somorjai, G. A.; Contreras, A. M.; Montano, M.; Rioux, R. M. *Proc. Natl. Acad. Sci. U.S.A.* **2006**, *103*, 10577.
- (2) Ertl, G.; Knözinger, H.; Weitkamp, J. *Handbook of Heterogeneous Catalysis*; VCH: Weinheim, 1997.
- (3) Bell, A. T. *Science* **2003**, *299*, 1688.
- (4) Burda, C.; Chen, X.; Narayanan, R.; El-Sayed, M. A. *Chem. Rev.* **2005**, *105*, 1025.
- (5) Chen, M.; Goodman, D. W. *Acc. Chem. Res.* **2006**, *39*, 739.
- (6) Crooks, R. M.; Zhao, M.; Sun, L.; Chechik, V.; Yeung, L. K. *Acc. Chem. Res.* **2001**, *34*, 181.
- (7) Lewis, L. N. *Chem. Rev.* **1993**, *93*, 2693.
- (8) Astruc, D.; Lu, F.; Aranzas, J. R. *Angew. Chem., Int. Ed.* **2005**, *44*, 7852.
- (9) Roucoux, A.; Schulz, J.; Patin, H. *Chem. Rev.* **2002**, *102*, 3757.
- (10) *Nanoparticles: From Theory To Application*; Schmid, G., Ed.; Wiley-VCH Verlag GmbH & Co. KGaA: Weinheim, 2004.
- (11) Wasylenko, W.; Frei, H. *Phys. Chem. Chem. Phys.* **2007**, *9*, 5497.
- (12) Kung, M. C.; Davis, R. J.; Kung, H. H. *J. Phys. Chem. C* **2007**, *111*, 11767.

- (13) Somorjai, G. A.; Park, J. Y. *Angew. Chem., Int. Ed.* **2008**, *47*, 9212.
- (14) Wilson, O. M.; Knecht, M. R.; Garcia-Martinez, J. C.; Crooks, R. M. *J. Am. Chem. Soc.* **2006**, *128*, 4510.
- (15) Freund, P.; Spiro, M. *J. Phys. Chem.* **1985**, *89*, 1074.
- (16) Bezemer, G. L.; Bitter, J. H.; Kuipers, H. P. C. E.; Oosterbeek, H.; Hollewijn, J. E.; Xu, X.; Kapteijn, F.; van Dillen, A. J.; de Jong, K. P. *J. Am. Chem. Soc.* **2006**, *128*, 3956.
- (17) Grass, M. E.; Rioux, R. M.; Somorjai, G. A. *Catal. Lett.* **2009**, *128*, 1–8.
- (18) Doyle, A. M.; Shaikhutdinov, S. K.; Freund, H.-J. *Angew. Chem., Int. Ed.* **2005**, *44*, 629.
- (19) van Santen, R. A. *Acc. Chem. Res.* **2009**, *42*, 57.
- (20) Che, M.; Bennett, C. O. *Adv. Catal.* **1989**, *36*, 55.
- (21) Honkala, K.; Helleman, A.; Remediakis, I. N.; Logadottir, A.; Carlsson, A.; Dahl, S.; Christensen, C. H.; Nørskov, J. K. *Science* **2005**, *307*, 555.
- (22) Topsoe, H. N. T. N.; Bohlbro, H.; Dumesic, A. Supported iron catalysts: particle size dependence of catalytic and chemisorptive properties. In *Studies in Surface Science and Catalysis 7a: Proceeding of the 7th International Congress on Catalysis*; Seiyama, T., Tanabe, K., Eds.; Elsevier: Amsterdam, 1981; p 247.
- (23) Henry, C. C. C.; Giorgio, S.; Goyhenex, C. Size effect in heterogeneous catalysis: A surface science approach. In *Chemisorption and Reactivity on Supported Clusters and Thin Films*; Lambert, R. M., Pacchioni, G., Eds.; Kluwer Academic: Dordrecht, The Netherlands, 1997; p 117.
- (24) Boudart, M. *Djega-Mariadassou Kinetics of Heterogeneous Catalytic Reactions*; Princeton University Press: Princeton, NJ, 1984.
- (25) Sau, T. K.; Pal, A.; Pal, T. J. *Phys. Chem. B* **2001**, *105*, 9266.
- (26) Deng, J.-P.; Shih, W.-C.; Mou, C.-Y. *ChemPhysChem* **2005**, *6*, 2021.

preparing monodisperse populations of nanoparticles of variable sizes and examining their catalytic properties, researchers have obtained tremendous insights into the size effect of heterogeneous catalysis at nanoscale. Recent technical advances have also made it possible to study nanoparticle catalysis at the single-particle level. Electrochemical measurements,<sup>27–33</sup> electrogenerated chemiluminescence,<sup>34</sup> surface plasmon resonance,<sup>35</sup> and fluorescence microscopy<sup>36–40</sup> have been used to detect catalytic reactions of individual nanoparticles. By removing ensemble averaging, single-particle measurements can uncover heterogeneous and dynamic behaviors of individual nanoparticles that are often hidden in averaged measurements.<sup>36–39</sup>

Our group developed a single-molecule fluorescence approach to study the catalysis of individual nanoparticles in real time.<sup>36–39</sup> By detecting the fluorescent product resorufin from the catalytic reduction of resazurin by  $\text{NH}_2\text{OH}$  at the single-molecule level, we monitored the catalysis of individual spherical 6 nm Au-nanoparticles at single-turnover resolution under ambient solution conditions (Figure 1A and Scheme S1 in Supporting Information). The single-turnover resolution measurements enabled us to separate cleanly the kinetics of the catalytic product formation reaction and the product dissociation reaction, and to determine the underlying kinetic mechanism. Under saturating  $\text{NH}_2\text{OH}$  concentrations, the catalytic product formation reaction follows a Langmuir–Hinshelwood mechanism, in which a Au-nanoparticle maintains a fast adsorption equilibrium of the substrate resazurin before a resazurin molecule is converted to the product resorufin on the nanoparticle surface (Figure 1B, reaction i). For the dissociation reaction of the product resorufin, two parallel reaction pathways exist: one a substrate-assisted pathway, in which the nanoparticle binds a substrate resazurin first before the product resorufin leaves the nanoparticle surface (reactions ii and iii), and the other a direct dissociation pathway (reaction iv). Between these two parallel reaction pathways, individual Au-nanoparticles show differential reactivity (i.e., different relative magnitudes between the two dissociation rate constants,  $k_2$  and  $k_3$ , for reactions iii and iv), resulting in three types of kinetic behaviors in the product dissociation reaction. This differential reactivity between parallel reaction pathways is fundamentally related to selectivity. (Selectivity is usually used for differential reactivity between parallel catalytic conversion reactions. Here, we have generalized its concept and applied it to parallel product dissociation reactions.) Furthermore, the activity of each nanoparticle shows large temporal fluctuations, attributable to both catalysis-induced

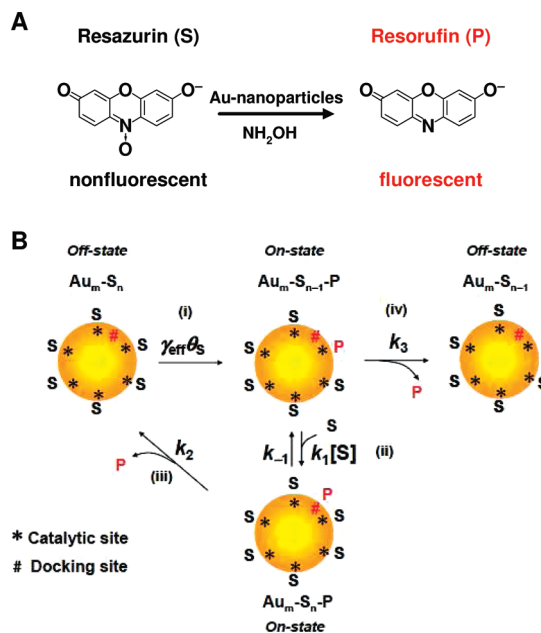


**Figure 1.** (A) Au-nanoparticle-catalyzed reduction of resazurin to resorufin by  $\text{NH}_2\text{OH}$  in aqueous solution. (B) Kinetic mechanism of catalysis.  $\text{Au}_m$ , Au-nanoparticle; S, the substrate resazurin; P, the product resorufin; [S], substrate concentration.  $\text{Au}_m\text{-S}_n$  represents a Au-nanoparticle having  $n$  adsorbed substrate molecules. The fluorescence state (on or off) of the nanoparticle is indicated at each reaction stage.  $\gamma_{\text{eff}} = k_{\text{T}}$  and represents the combined reactivity of all surface catalytic sites of a nanoparticle.  $k$  is a rate constant representing the reactivity per catalytic site for the catalytic conversion.  $n_{\text{T}}$  is the total number of surface catalytic sites on one Au-nanoparticle.  $\theta_{\text{S}}$  is the fraction of catalytic sites that are occupied by substrates and equals  $K_1[S]/(1 + K_1[S])$ , where  $K_1$  is the substrate adsorption equilibrium constant. This kinetic mechanism is formulated at saturating concentrations of the cosubstrate  $\text{NH}_2\text{OH}$ , whose contribution is included in  $k$  implicitly.<sup>36</sup> Part (B) adapted from Xu et al.<sup>36</sup>

and spontaneous dynamic surface restructuring of the nanoparticle. Although this dynamic surface restructuring has yet to be observed directly, its time scale can be determined by analyzing the clear activity fluctuations of individual nanoparticles. For the Au-nanoparticles we studied, the time scales of dynamic surface restructuring show large variations from one nanoparticle to another.

As the catalytic properties of nanoparticles depend on their size, nanoparticles of different sizes are expected to have different catalytic activity and possibly different selectivity. The dynamic surface restructuring of nanoparticles should also depend on their size: smaller nanoparticles have higher surface energies and thus should be more prone to surface reconstruction, which can lead to different catalytic dynamics for different-sized nanoparticles. To probe systematically how size affects the catalytic activity and dynamics of Au-nanoparticles at the single-molecule level, here we study the catalysis of individual spherical Au-nanoparticles of  $9.1 \pm 1.5$  and  $13.7 \pm 2.4$  nm diameters (Figure S1), in correlation with our previous study of  $6.0 \pm 1.7$  nm diameter Au-nanoparticles.<sup>36–39</sup> (We also examined the 2 nm Au-nanoparticles from Ted Pella. They are inactive in catalyzing the reduction of resazurin to resorufin by  $\text{NH}_2\text{OH}$ , likely due to deactivation by thiocyanate that was used in the synthesis to stabilize the nanoparticles of this small size (Communication with British Biocell International/Ted Pella).) We examine the size dependence of their activity in both the catalytic product formation reaction and the product dissociation reaction, of their selectivity in the two parallel product dissociation pathways, and of their surface-restructuring-coupled

- (27) Tel-Vered, R.; Bard, A. J. *J. Phys. Chem. B* **2006**, *110*, 25279.  
 (28) Xiao, X.; Bard, A. J. *J. Am. Chem. Soc.* **2007**, *129*, 9610.  
 (29) Krapf, D.; Wu, M.-Y.; Smeets, R. M. M.; Zandbergen, H. W.; Dekker, C.; Lemay, S. G. *Nano Lett.* **2006**, *6*, 105.  
 (30) Chen, S.; Kucernak, A. *J. Phys. Chem. B* **2004**, *108*, 13984.  
 (31) Chen, S.; Kucernak, A. *J. Phys. Chem. B* **2003**, *107*, 8392.  
 (32) Meier, J.; Friedrich, K. A.; Stimming, U. *Faraday Discuss.* **2002**, *121*, 365.  
 (33) Meier, J.; Schiott, J.; Liu, P.; Norskov, J. K.; Stimming, U. *Chem. Phys. Lett.* **2004**, *390*, 440.  
 (34) Fan, F.-R. F.; Bard, A. J. *Nano Lett.* **2008**, *8*, 1746.  
 (35) Novo, C.; Funston, A. M.; Mulvaney, P. *Nat. Nanotechnol.* **2008**, *3*, 598.  
 (36) Xu, W.; Kong, J. S.; Yeh, Y.-T. E.; Chen, P. *Nat. Mater.* **2008**, *7*, 992.  
 (37) Xu, W.; Kong, J. S.; Chen, P. *J. Phys. Chem. C* **2009**, *113*, 2393.  
 (38) Xu, W.; Kong, J. S.; Chen, P. *Phys. Chem. Chem. Phys.* **2009**, *11*, 2767.  
 (39) Chen, P.; Xu, W.; Zhou, X.; Panda, D.; Kalininskiy, A. *Chem. Phys. Lett.* **2009**, *470*, 151.  
 (40) Sakamoto, M.; Tachikawa, T.; Fujitsuka, M.; Majima, T. *J. Am. Chem. Soc.* **2009**, *131*, 6–7.

catalytic dynamics. We also use simple thermodynamic models to analyze quantitatively their size-dependent properties.

## 2. Experimental Methods

**Materials and Characterizations.** All commercial materials were used as received unless specified. The three different-sized Au-nanoparticles, prepared from citrate reduction of HAuCl<sub>4</sub> in aqueous solutions, were purchased from British Biocell International/Ted Pella and characterized by TEM (FEI Tecnai 12) at the Cornell Center for Materials Research. TEM images and size distributions of these nanoparticles are shown in Figure S1; their diameters are  $6.0 \pm 1.7$ ,  $9.1 \pm 1.5$ , and  $13.7 \pm 2.4$  nm.

**Single-Molecule Imaging Experiments and Analyses.** A flow cell,  $100 \mu\text{m}$  (height)  $\times$   $2$  cm (length)  $\times$   $5$  mm (width), formed by double-sided tapes sandwiched between a quartz slide (Technical Glass) and a borosilicate coverslip (Gold Seal), was used to hold aqueous reactant solutions for single-molecule fluorescence measurements. The quartz slide was amine-functionalized by an aminoalkylsiloxane reagent (Vectabond, Vector Laboratory) to have a positively charged surface to immobilize the negatively charged Au-nanoparticles.<sup>41–43</sup> Reactant solutions were supplied in continuous flow at  $5 \mu\text{L min}^{-1}$  using a syringe pump. All single-molecule imaging experiments of nanoparticle catalysis were carried out at room temperature with a saturating NH<sub>2</sub>OH concentration of  $1$  mM at neutral pH.

Single-molecule fluorescence measurements were performed as previously described,<sup>36,38</sup> using a home-built prism-type total internal reflection fluorescence microscope (Olympus IX71). A continuous wave circularly polarized  $532$  nm laser beam (Crysta-Laser) of  $2$ – $6$  mW was focused onto an area of  $\sim 50 \times 90 \mu\text{m}^2$  on the sample to directly excite the fluorescence of resorufin. The fluorescence was collected by a  $60\times$  NA1.2 water-immersion objective, filtered, and detected by an ANDOR Ixon EMCCD camera operated at  $50$  ms frame rate. An additional  $1.6\times$  magnification on the microscope is also used sometimes. The movies were analyzed to extract out the fluorescence intensity trajectories from localized fluorescence spots individually across the entire movie. The waiting times were extracted from the trajectories via threshold analysis and statistically analyzed.

## 3. Results and Analyses

### 3.1. Size-Dependent Catalytic Activity of Au-Nanoparticles.

Using single-molecule fluorescence microscopy (Scheme S1) and following the fluorescence signal of the catalytic product resorufin (Figure 1A), we studied the catalysis of individual  $9.1$  and  $13.7$  nm Au-nanoparticles. Figure 2A and Figure S2 show exemplary fluorescence turnover trajectories of a single  $9.1$  nm and a single  $13.7$  nm Au-nanoparticle. The digital nature of the stochastic off-on fluorescence bursts and the consistent height of the on-level are characteristic of single-molecule fluorescence detection. Each sudden intensity increase here marks a formation of a product resorufin on the nanoparticle; each intensity decrease marks a dissociation of the product from the nanoparticle; and each off–on cycle corresponds to a single turnover of catalytic formation of a product on one nanoparticle and its subsequent dissociation. The actual chemical transformations occur at subpicosecond time scale and cannot be resolved in

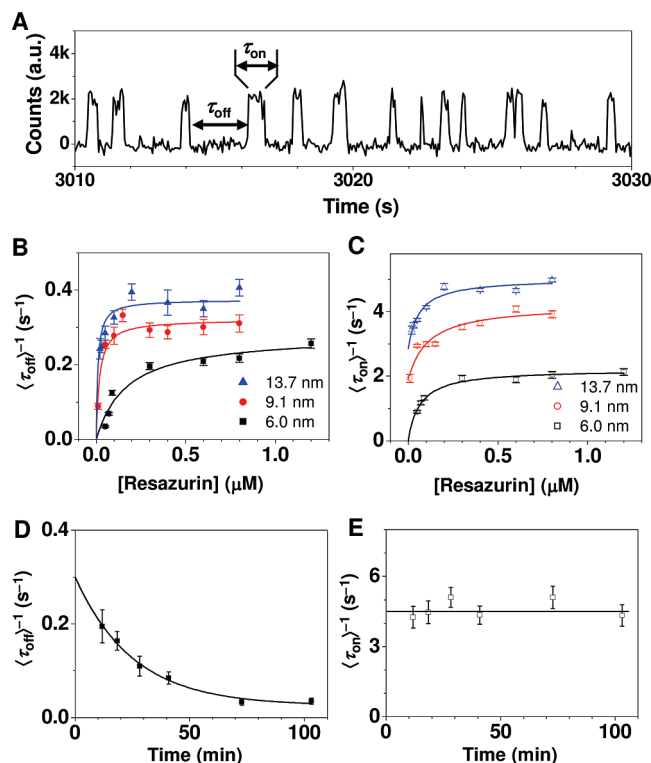


**Figure 2.** (A) Segment of the fluorescence turnover trajectory of a single  $9.1$  nm Au-nanoparticle at  $0.3 \mu\text{M}$  resazurin,  $1$  mM NH<sub>2</sub>OH, and  $50$  ms imaging rate. au = arbitrary units. (B,C) Resazurin concentration titrations of  $\langle\tau_{\text{off}}\rangle^{-1}$  and  $\langle\tau_{\text{on}}\rangle^{-1}$  of  $6.0$ ,  $9.1$ , and  $13.7$  nm Au-nanoparticles. Each data point is averaged over the turnover trajectories of  $>50$  nanoparticles, with sem as the error bar. Solid lines are fits with eqs 1a and 1b; the fitting parameters are summarized in Table 1. Data of  $6.0$  nm from Xu et al.<sup>36</sup> (D,E) Time profiles of  $\langle\tau_{\text{off}}\rangle^{-1}$  and  $\langle\tau_{\text{on}}\rangle^{-1}$  from the fluorescence turnover trajectory of a single  $9.1$  nm Au-nanoparticle at  $0.6 \mu\text{M}$  resazurin and  $1$  mM NH<sub>2</sub>OH. Each data point is an average of tens of turnovers, and the error bar is sem. The solid line in (D) is a fit with the exponential function  $\langle\tau_{\text{off}}\rangle^{-1} = ae^{-t/c} + b$ , and the fitted value at  $t = 0$  is used for this resazurin concentration for determining the titration curves in (B).

these single-molecule fluorescence trajectories. Once the product resorufin leaves the nanoparticle surface, it becomes undetectable at our imaging rate ( $50$  ms/frame) because of its fast diffusion in solution. Under our laser excitation intensities, the photobleaching or blinking of the product resorufin is insignificant, as compared to its residence time on a nanoparticle.<sup>36</sup>

In these fluorescence turnover trajectories, the two stochastic waiting times,  $\tau_{\text{off}}$  and  $\tau_{\text{on}}$ , carry the information of reaction kinetics:  $\tau_{\text{off}}$  is the waiting time before each product formation,  $\tau_{\text{on}}$  is the waiting time for product dissociation after its formation, and resolving them enables examining the kinetics of catalytic product formation and product dissociation reactions separately. Based on the mechanism in Figure 1B,  $\langle\tau_{\text{off}}\rangle^{-1}$ , the time-averaged single-particle rate of product formation ( $\langle \rangle$  denotes averaging), and  $\langle\tau_{\text{on}}\rangle^{-1}$ , the time-averaged single-particle rate of product dissociation, are connected with the conventional kinetic parameters as:<sup>36,37</sup>

$$\langle\tau_{\text{off}}\rangle^{-1} = \frac{\gamma_{\text{eff}}K_1[S]}{1 + K_1[S]} \quad (1a)$$

$$\langle\tau_{\text{on}}\rangle^{-1} = \frac{k_2K_2[S] + k_3}{1 + K_2[S]} \quad (1b)$$

Here,  $[S]$  is the concentration of the substrate resazurin; the kinetic parameters are defined in Figure 1B and its caption; and

(41) Handley, D. A. Methods for Synthesis of Colloid Gold. In *Colloidal Gold: Principles, Methods, and Applications*; Hayat, M. A., Ed.; Academic Press, Inc.: San Diego, CA, 1989; Vol. 1, p 13.

(42) Natan, M. J.; Lyon, L. A. Surface Plasmon Resonance Biosensing with Colloidal Au Application. In *Metal Nanoparticles: Synthesis, Characterization, and Application*; Feldheim, D. L., Foss, C. A., Jr., Eds.; Marcel Dekker, Inc.: New York, 2002; p 183.

(43) Grabar, K. C.; Freeman, R. G.; Hommer, M. B.; Natan, M. J. *Anal. Chem.* **1995**, *67*, 735.

**Table 1.** Nanoparticle-Averaged Kinetic Parameters of Spherical Au-Nanoparticles of Different Diameters ( $d$ ) and Extrapolated Bulk Values from Thermodynamic Analysis

$d$ (nm)	$\gamma_{\text{eff}}$ ( $\text{s}^{-1}$ )	$(\gamma_{\text{eff}}/A) \times 10^3$ ( $\text{s}^{-1} \text{nm}^{-2}$ )	$K_1$ ( $\mu\text{M}^{-1}$ )	$k_2$ ( $\text{s}^{-1}$ )	$k_3$ ( $\text{s}^{-1}$ )	$K_2$ ( $\mu\text{M}^{-1}$ )
6.0 $\pm$ 1.7	0.28 $\pm$ 0.02	2.5 $\pm$ 0.9	6 $\pm$ 2	2.2 $\pm$ 0.1	0 $\pm$ 3	16 $\pm$ 2
9.1 $\pm$ 1.5	0.32 $\pm$ 0.01	1.2 $\pm$ 0.2	57 $\pm$ 7	4.2 $\pm$ 0.3	1.9 $\pm$ 0.3	9.4 $\pm$ 0.2
13.7 $\pm$ 2.4	0.37 $\pm$ 0.02	0.6 $\pm$ 0.1	110 $\pm$ 5	5.0 $\pm$ 0.2	2.9 $\pm$ 0.4	16.3 $\pm$ 0.1
bulk <sup>a</sup>		0.18 $\pm$ 0.03	600 $\pm$ 50	11 $\pm$ 3	17 $\pm$ 3	
Brønsted–Polanyi parameters		$\alpha_{\text{cat}} = 0.23 \pm 0.05$		$\alpha_{\text{ads}} = 0.4 \pm 0.1^b$	$\alpha_{\text{ads}} = 1 \pm 0.6^b$	

<sup>a</sup> The values of bulk gold were obtained by fitting the size dependence of each kinetic parameter in Figure 5. <sup>b</sup> The  $\alpha_{\text{ads}}$ 's are the Brønsted–Polanyi parameters for the rate constants of corresponding adsorption reactions, that is, the reverse reactions of  $k_2$  and  $k_3$ .

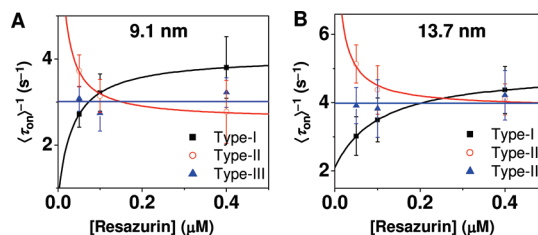
$K_2 = k_1/(k_{-1} + k_2)$ . At saturating resazurin concentrations,  $\langle\tau_{\text{off}}\rangle^{-1}$  equals  $\gamma_{\text{eff}}$ , the single-particle catalytic rate constant that represents the combined reactivity of all surface catalytic sites, and  $\langle\tau_{\text{on}}\rangle^{-1}$  equals  $k_2$ , the product dissociation rate constant in the substrate-assisted pathway (Figure 1B).

Figure 2B and C show the resazurin concentration titration curves of  $\langle\tau_{\text{off}}\rangle^{-1}$  and  $\langle\tau_{\text{on}}\rangle^{-1}$  for 6.0, 9.1, and 13.7 nm Au-nanoparticles, each curve averaged over many nanoparticles. For each 9.1 or 13.7 nm nanoparticle, we observed a time-dependent exponential decay of  $\langle\tau_{\text{off}}\rangle^{-1}$  over tens of minutes time scale at all resazurin concentrations, although its  $\langle\tau_{\text{on}}\rangle^{-1}$  does not show this decay behavior (Figure 2D,E and Figure S3). This temporal decay of  $\langle\tau_{\text{off}}\rangle^{-1}$  indicates a catalytic deactivation of these Au-nanoparticles. This deactivation is possibly in part due to poisoning by reaction products such as oxidation products of  $\text{NH}_2\text{OH}$ , but likely not by the product resorufin because  $\langle\tau_{\text{on}}\rangle^{-1}$ , the resorufin dissociation rate, does not decay over time. To compensate for this catalytic deactivation for each nanoparticle of these two sizes, we fitted its time profile of  $\langle\tau_{\text{off}}\rangle^{-1}$  with an exponential function to obtain its initial value at each resazurin concentration for determining the titration curves in Figure 2B. In contrast to 9.1 and 13.7 nm particles, deactivation for 6 nm Au-nanoparticles only becomes noticeable after about 3 h,<sup>36</sup> we have thus limited our analyses of 6 nm particles to data collected within 3 h of reaction time.

All three different-sized Au-nanoparticles show saturation kinetics of  $\langle\tau_{\text{off}}\rangle^{-1}$  and  $\langle\tau_{\text{on}}\rangle^{-1}$  with increasing  $[\text{S}]$ , as predicted by eqs 1a and 1b (Figure 2B,C). Clear differences also exist: with decreasing size, the saturation levels decrease for both  $\langle\tau_{\text{off}}\rangle^{-1}$  and  $\langle\tau_{\text{on}}\rangle^{-1}$ , indicating smaller  $\gamma_{\text{eff}}$  and  $k_2$  for smaller nanoparticles (see below). Fitting the  $[\text{S}]$  titration curves with eqs 1a and 1b gives the kinetic parameters of the Au-nanoparticles (Table 1).

The kinetic parameters show clear size-dependent catalytic activity of Au-nanoparticles across the three sizes (Table 1). For the catalytic product formation reaction,  $\gamma_{\text{eff}}$ , the single-particle catalytic rate constant, decreases with decreasing size, indicating the lower catalytic reactivity per particle for smaller nanoparticles. This decrease of  $\gamma_{\text{eff}}$  mainly results from the smaller surface area (i.e., fewer surface catalytic sites) of the smaller nanoparticles, because the catalytic reactivity per surface area,  $\gamma_{\text{eff}}/A$  ( $A$  is the nanoparticle surface area), increases with decreasing size. This increase in reactivity per surface area reports the higher catalytic reactivity per catalytic site for smaller nanoparticles and is accompanied by a decrease of substrate adsorption equilibrium constant at each site ( $K_1$ ). Therefore, for the Au-nanoparticles studied here, higher catalytic reactivity is correlated with weaker substrate binding to the catalytic site.

The weaker binding of substrate resazurin to smaller Au-nanoparticles is surprising, as smaller particles typically bind adsorbates stronger because of the greater coordination unsaturation of their surface atoms. A possible reason here is that



**Figure 3.** Resazurin concentration titrations of  $\langle\tau_{\text{on}}\rangle^{-1}$  of individual 9.1 nm (A) and 13.7 nm (B) Au-nanoparticles showing type I, II, and III kinetic behaviors. The solid lines are fits with eq 1b, with parameters summarized in Table S1.

the substrate resazurin binds to the Au-nanoparticle with its aromatic ring parallel to the surface; this binding mode would prefer larger particles that have larger surface terraces.

For the product dissociation reaction, the rate constants of both the substrate-assisted dissociation pathway ( $k_2$ ) and the direct dissociation pathway ( $k_3$ ) decrease with decreasing particle size. These decreases in product dissociation rate constants suggest a stronger binding of the product resorufin to the nanoparticle surface, in contrast with the weaker binding of the substrate resazurin, for smaller nanoparticles.

**3.2. Size-Dependent Selectivity in Parallel Product Dissociation Pathways.** For the Au-nanoparticle-catalyzed resazurin reduction to resorufin, the dissociation of the product resorufin has two parallel reaction pathways (Figure 1B): one a substrate-assisted pathway and the other a direct dissociation pathway. For a single Au-nanoparticle, it can have differential selectivity between these two parallel reaction pathways, which is manifested by the  $[\text{S}]$  dependence of its  $\langle\tau_{\text{on}}\rangle^{-1}$ . From eq 1b, when  $[\text{S}] \rightarrow 0$ ,  $\langle\tau_{\text{on}}\rangle^{-1} = k_3$ , that is, the direct product dissociation dominates; when  $[\text{S}] \rightarrow \infty$ ,  $\langle\tau_{\text{on}}\rangle^{-1} = k_2$ , that is, the high  $[\text{S}]$  drives the product dissociation to the substrate-assisted pathway. If  $k_2$  and  $k_3$ , the product dissociation rate constants in these two pathways, differ in their relative magnitudes,  $\langle\tau_{\text{on}}\rangle^{-1}$  will have three types of kinetic behaviors: (I) asymptotic increase with increasing  $[\text{S}]$  if the nanoparticle has  $k_2 > k_3$ ; that is, the nanoparticle prefers the substrate-assisted dissociation pathway; (II) asymptotic decrease if  $k_2 < k_3$ ; that is, the nanoparticle prefers the direct dissociation pathway; and (III) constant at any  $[\text{S}]$  if  $k_2 = k_3$ ; that is, the nanoparticle takes the two pathways equally, or if  $K_2 = 0$ . Our single-particle measurements enable the examination of these different kinetic behaviors, and all three types were observed previously for 6.0 nm Au-nanoparticles: 66% of 6.0 nm Au-nanoparticles show type I behavior, 19% show type II, and 15% show type III.<sup>36</sup>

These three types of kinetic behaviors of  $\langle\tau_{\text{on}}\rangle^{-1}$  are also observed for the 9.1 and 13.7 nm Au-nanoparticles. Figure 3 gives exemplary  $[\text{S}]$  titrations of  $\langle\tau_{\text{on}}\rangle^{-1}$  of single 9.1 and 13.7 nm Au-nanoparticles. Strikingly, as compared to the 6.0 nm Au-nanoparticles, the relative subpopulations shifted among the

**Table 2.** Size-Dependent Relative Subpopulations of Type I, II, and III Kinetic Behaviors<sup>a</sup>

$d$ (nm)	type I ( $k_2 > k_3$ )	type II ( $k_2 < k_3$ )	type III ( $k_2 \approx k_3$ )
6.0	66%	19%	15%
9.1	66%	11%	23%
13.7	43%	6%	51%

<sup>a</sup> Tens to hundreds of nanoparticles were analyzed for each size. Data of 6.0 nm from Xu et al.<sup>36</sup>

three types of kinetic behaviors (Table 2): with increasing size, the subpopulations of type I and II behaviors decrease, while that of type III increases. As type III particles have nearly equal reactivity in the two parallel product dissociation pathways (i.e.,  $k_2 \approx k_3$ ), the increase in their subpopulation indicates that larger Au-nanoparticles are less selective in the product dissociation reaction. Our previous studies have shown that  $k_2$  and  $k_3$  are the rate constants of product dissociation at the docking sites and the catalytic sites, respectively (Figure 1B);<sup>36,38</sup> therefore, the increased subpopulation of type III behavior for larger particles suggests that their catalytic sites and docking sites become more alike in their kinetic properties. Combined with the results in section 3.1, this subpopulation shift among the three types of kinetic behaviors across the different particle sizes demonstrates that tuning nanoparticle size can tune reaction selectivity, besides tuning activity.

**3.3. Size-Dependent Catalytic Dynamics.** Because of their nanometer size, the surfaces of nanoparticles are unstable and can reconstruct dynamically, especially under catalysis, where the constantly changing adsorbate–surface interactions can further induce dynamic surface restructuring.<sup>13,44–49</sup> These surface structural dynamics can cause temporal dynamics of catalytic activity of individual nanoparticles: the activity of a nanoparticle fluctuates over time, and the fluctuation correlation time is the time scale of the underlying surface restructuring. Experimentally, one manifestation of this temporal activity fluctuation is the temporal variation of a nanoparticle's rate of turnovers (the number of fluorescence off–on cycles per unit time), as observed in our previous study of 6.0 nm Au-nanoparticles.<sup>36,38</sup>

For each nanoparticle, the temporal variation of its rate of turnovers has contributions from the reaction rate changes in both the  $\tau_{\text{off}}$  reaction (the catalytic product formation) and the  $\tau_{\text{on}}$  reaction (the product dissociation). These two contributions can be evaluated separately for each nanoparticle by extracting the sequences of individual  $\tau_{\text{off}}$  and  $\tau_{\text{on}}$  from its turnover trajectory and analyzing their autocorrelation functions  $C_\tau(m) = \langle \Delta\tau(0)\Delta\tau(m) \rangle / \langle \Delta\tau^2 \rangle$ .<sup>36,39,50,51</sup> Here,  $\tau$  is either  $\tau_{\text{off}}$  or  $\tau_{\text{on}}$ ,  $m$  is the turnover index number in the sequences, and  $\Delta\tau(m) = \tau(m) - \langle \tau \rangle$ . In the presence of activity fluctuations,  $C_\tau(m) \geq 0$ , and shows a decay behavior with the decay time constant being the activity fluctuation correlation time.

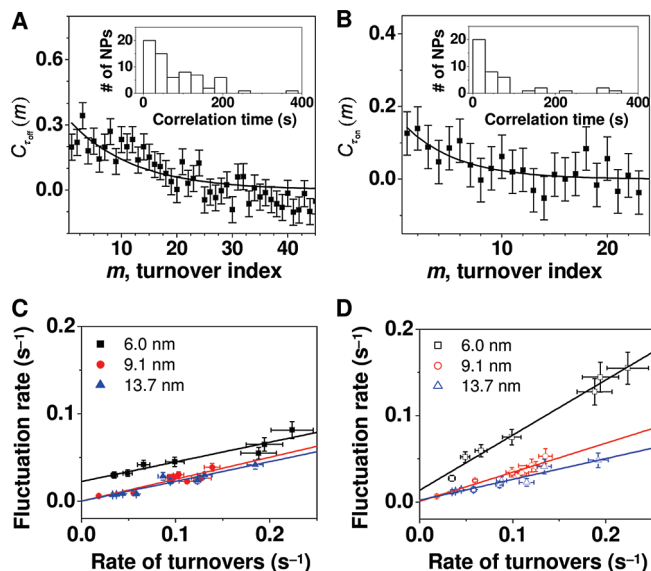


**Figure 4.** (A,B) Autocorrelation functions of the  $\tau_{\text{off}}$  (A) and  $\tau_{\text{on}}$  (B) from the turnover trajectory of a single 9.1 nm Au-nanoparticle at 0.8  $\mu\text{M}$  resazurin. Solid lines are exponential fits with decay constants of  $m_{\text{off}} = 11.6 \pm 0.8$  and  $m_{\text{on}} = 5.0 \pm 0.4$  turnovers. Inset: Histograms of fluctuation correlation times for  $\tau_{\text{off}}$  and  $\tau_{\text{on}}$  reactions at 0.8  $\mu\text{M}$  resazurin. NPs: nanoparticles. (C,D) Dependence of the activity fluctuation rate (the inverse of fluctuation correlation time) of the  $\tau_{\text{off}}$  reaction (C) and the  $\tau_{\text{on}}$  reaction (D) on the rate of turnovers. Each data point is an average from >50 trajectories. Error bars are sem. Solid lines are linear fits. Fitting parameters are summarized in Table S2. Data of 6.0 nm from Xu et al.<sup>36</sup>

Figure 4A,B shows exemplary  $C_{\tau_{\text{off}}}(m)$  and  $C_{\tau_{\text{on}}}(m)$  of a single 9.1 nm Au-nanoparticle, and Figure S4 shows those of a single 13.7 nm Au-nanoparticle. The exponential decay behaviors of  $C_{\tau_{\text{off}}}(m)$  and  $C_{\tau_{\text{on}}}(m)$  directly demonstrate the activity fluctuations in the catalytic product formation and the product dissociation reaction, respectively. For the 9.1 nm Au-nanoparticle in Figure 4A and B, the exponential decay constant of  $C_{\tau_{\text{off}}}(m)$  is  $m_{\text{off}} = 11.6 \pm 0.8$  turnovers, and that of  $C_{\tau_{\text{on}}}(m)$  is  $m_{\text{on}} = 5.0 \pm 0.4$  turnovers. With an average turnover time of  $\sim 14.2$  s for this particular nanoparticle, the activity fluctuation correlation times for its  $\tau_{\text{off}}$  and  $\tau_{\text{on}}$  reactions are  $\sim 165$  and  $\sim 71$  s, respectively. These two correlation times are the time scales of the dynamic surface restructuring at the respective surface sites where the  $\tau_{\text{off}}$  and  $\tau_{\text{on}}$  reactions take place on this nanoparticle. Moreover, similar to 6.0 nm Au-nanoparticles,<sup>36</sup> the distributions of the fluctuation correlation time are broad for both 9.1 and 13.7 nm nanoparticles (Figure 4A,B insets, and Figure S4 insets), indicating that individual nanoparticles can have very different surface restructuring time scales.

The catalysis-induced nature of the activity fluctuations and the underlying surface restructuring are directly supported by the positive correlation between the activity fluctuation rates (i.e., the inverse of fluctuation correlation times) and the rate of turnovers. For all three sizes of Au-nanoparticles, the activity fluctuation rates increase with increasing rates of turnovers (Figure 4C,D), following an approximate linear correlation. At any rates of turnovers, the activity fluctuation rates of both  $\tau_{\text{off}}$  and  $\tau_{\text{on}}$  reactions are higher for the smaller Au-nanoparticles than for the larger Au-nanoparticles. This size dependence indicates that the catalysis-induced dynamic surface restructuring becomes faster with decreasing particle size.

The activity fluctuation rates can be extrapolated linearly to zero rate of turnovers for all three sizes of Au-nanoparticles. The positive intercepts approximate the rates of spontaneous

(44) Somorjai, G. A. *Introduction to Surface Chemistry and Catalysis*; Wiley-Interscience: New York, 1994.

(45) Imbihl, R.; Ertl, G. *Chem. Rev.* **1995**, *95*, 697.

(46) *Phase Transitions and Adsorbate Restructuring at Metal Surfaces*; King, D. A., Woodruff, D. P., Eds.; Elsevier Science: New York, 1994.

(47) Tao, F.; Grass, M. E.; Zhang, Y.; Butcher, D. R.; Renzas, J. R.; Liu, Z.; Jen; Chung, Y.; Mun, B. S.; Salmeron, M.; Somorjai, G. A. *Science* **2008**, *322*, 932.

(48) Hansen, P. L.; Wagner, J. B.; Helveg, S.; Rostrup-Nielsen, J. R.; Clausen, B. S.; Topsoe, H. *Science* **2002**, *295*, 2053.

(49) Newton, M. A.; Belver-Coldeira, C.; Martinez-Arias, A.; Fernandez-Garcia, M. *Nat. Mater.* **2007**, *6*, 528.

(50) Lu, H. P.; Xun, L. Y.; Xie, X. S. *Science* **1998**, *282*, 1877.

(51) Witkoskie, J. B.; Cao, J. J. *Chem. Phys.* **2004**, *121*, 6361.

(as compared to catalysis-induced) dynamic surface restructuring for a Au-nanoparticle in an aqueous environment, corresponding to a time scale of tens to hundreds of seconds (Figure 4C,D). Moreover, the intercepts are higher for smaller Au-nanoparticles, indicating their faster spontaneous dynamic surface restructuring. This faster spontaneous dynamic surface restructuring is consistent with that the surface atoms of smaller Au-nanoparticles are less stable and therefore more prone to reconstruction.

Real-time, direct observation of dynamic surface restructuring of nanoparticles is challenging, and we do not yet have direct experimental measurements. In our single-particle catalysis experiments, the dynamic surface restructuring is manifested by the resulted activity fluctuations of individual nanoparticles. The faster activity fluctuations for smaller particles further support dynamic surface restructuring as the underlying physical cause. The dynamic nature of Au-nanoparticle surfaces is also consistent with recent studies of bulk gold surfaces.<sup>52–54</sup>

**3.4. Effect of Stabilization Ligands.** The colloidal Au-nanoparticles studied here have citrate ions on their surfaces as stabilization ligands. Although these nanoparticles were extensively washed with water after immobilization on the quartz surface, residual citrate can still be present and may play roles in the catalysis and the dynamic surface restructuring. To probe the possible effects, we performed control catalysis experiments at both the ensemble and the single-particle level in the presence of varying concentrations of citrate. Up to concentrations much larger than the resazurin concentration, citrate has no significant effect on the catalytic conversion rate, the product dissociation rate, or the time scale of the activity fluctuations of Au-nanoparticles (Figures S5–S7). Therefore, citrate does not play important roles in catalysis and surface restructuring under our experimental conditions.

## 4. Discussion

We have applied single-molecule fluorescence microscopy to study the catalysis of different-sized Au-nanoparticles, focusing on the fluorogenic reaction of resazurin reduction to resorufin. The catalytic activity of Au-nanoparticles shows clear size dependence, as do their temporal catalytic dynamics that are attributable to the dynamic restructuring of nanoparticle surfaces. These size-dependent catalytic behaviors result fundamentally from the nanosize effect on the chemical properties of metal catalysts. On the structural side, the surface atoms of nanoparticles have greater coordination unsaturation,<sup>55</sup> which can lead to their different catalytic properties from bulk materials. On the thermodynamic side, nanoparticles have excess surface free energy as compared to bulk materials,<sup>56</sup> which can lead to their different energetics and kinetics for adsorbate binding and for catalytic conversions. This excess surface free energy also affects the cohesive energy of nanoparticles, influencing their surface restructuring that involves breaking or partial breaking of the bonding between surface atoms. In this section, we will use thermodynamic considerations to analyze quantitatively the size-dependent catalytic activity and dynamics

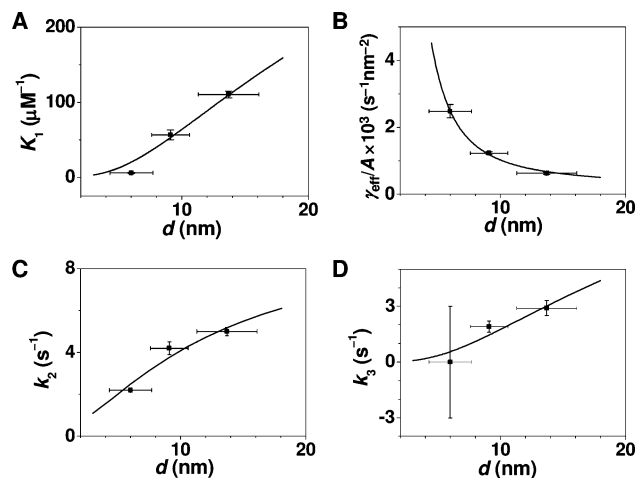


**Figure 5.** Thermodynamic analyses of the size dependence of kinetic parameters for Au-nanoparticle catalysis. Solid lines are fits with eqs 3 (A), 6 (B), and 8 (C,D). The thermodynamic parameters used for bulk gold are:  $\sigma_{\infty} = 1.54 \text{ J m}^{-2}$ ,<sup>65</sup>  $h = 0.270 \text{ nm}$ ,<sup>66</sup> and  $E_b = 367.4 \text{ kJ mol}^{-1}$ .<sup>67,68</sup> The bulk boiling temperature (3129 K)<sup>69</sup> is used for  $T_b$  as done previously.<sup>62–64</sup> Fitting results are summarized in Table 1.

of Au-nanoparticles. Below we first analyze the size-dependent catalytic activity. We then analyze the size-dependent kinetics and energetics of dynamic surface restructuring that gives the temporal catalytic dynamics of Au-nanoparticles.

### 4.1. Thermodynamic Analysis of Size-Dependent Activity.

The clean resolution of  $\tau_{\text{off}}$  and  $\tau_{\text{on}}$  in the fluorescence turnover trajectories of Au-nanoparticles allowed us to probe the size-dependent kinetics of the catalytic product formation reaction ( $\tau_{\text{off}}$ ) and the product dissociation reaction ( $\tau_{\text{on}}$ ) separately (section 3.1). A number of kinetic parameters show clear size dependence (Table 1), including  $K_1$ , the substrate adsorption equilibrium constant;  $\gamma_{\text{eff}}/A$ , the catalytic rate constant per surface area;  $k_2$ , the product dissociation rate constant in the substrate-assisted pathway; and  $k_3$ , the rate constant for direct product dissociation.

To analyze quantitatively the size-dependent activity of Au-nanoparticles, we use a classical thermodynamic formalism of Parmon and Murzin that approximates a metal nanoparticle as a continuous phase and attributes its size effect to changes in its chemical potential.<sup>57,58</sup> The changes in chemical potential and thus Gibbs free energy are then translated to changes in reaction kinetics through the Brønsted–Polanyi relation to derive the size-dependent kinetics. This treatment is applicable for particles containing more than  $\sim 100$  atoms, for which the energy level splitting of the particle is much smaller than the thermal energy and the quantum size effect is negligible.<sup>57</sup> For gold, this size regime encompasses particles of larger than  $\sim 2 \text{ nm}$  diameters, including the nanoparticles studied here.

With this thermodynamic formalism,<sup>57,58</sup> the Gibbs free energy of adsorption for a molecule interacting with a nanoparticle of diameter  $d$  is:

$$\Delta G_{\text{ads}}(d) = \Delta G_{\text{ads},\infty} \pm \delta(d) = \Delta G_{\text{ads},\infty} \pm 4\sigma V_M/d \quad (2)$$

Here,  $\Delta G_{\text{ads},\infty}$  is the adsorption free energy to the bulk material,  $\delta(d) = 4\sigma V_M/d$ , and accounts for the size-dependent chemical potential change,  $\sigma$  is the surface tension of the nanoparticle, and  $V_M$  is the partial molar volume of the nanoparticle. Depending on the nature of the bonding interactions of the

(52) Baber, A. E.; Jensen, S. C.; Iski, E. V.; Sykes, E. C. H. *J. Am. Chem. Soc.* **2006**, *128*, 15384–15385.

(53) Hrbek, J.; Hoffmann, F. M.; Park, J. B.; Liu, P.; Stacchiola, D.; Hoo, Y. S.; Ma, S.; Nambu, A.; Rodriguez, J. A.; White, M. G. *J. Am. Chem. Soc.* **2008**, *130*, 17272–17273.

(54) Gao, W.; Baker, T. A.; Zhou, L.; Pinnaduwa, D. S.; Kaxiras, E.; Friend, C. M. *J. Am. Chem. Soc.* **2008**, *130*, 3560–3565.

(55) Van Harveldt, R.; Hartog, F. *Surf. Sci.* **1969**, *15*, 189.

(56) Adamson, A. W.; Gast, A. P. *Physical Chemistry of Surfaces*, 6th ed.; John Wiley & Sons, Inc.: New York, 1997.

(57) Parmon, V. N. *Dokl. Phys. Chem.* **2007**, *413*, 42.

(58) Murzin, D. Y. *Chem. Eng. Sci.* **2009**, *64*, 1046.

molecule with the nanoparticle surface, the change in adsorption free energy from the nanosize effect can be positive or negative, as compared to that of the bulk material (here the bulk materials refer to particles with micrometer or larger diameters).<sup>57,58</sup>

**Catalytic Product Formation Reaction.** For the catalytic product formation reaction, the adsorption equilibrium constant of the substrate resazurin,  $K_1$ , decreases with decreasing particle size (Table 1 and Figure 5A), indicating a weakened adsorption to the Au-nanoparticle surface as compared to that to the bulk gold surface. Therefore, the adsorption of resazurin to the Au-nanoparticle surface corresponds to the case that the change in adsorption free energy from the nanosize effect is positive, that is,  $\Delta G_{\text{ads}}(d) = \Delta G_{\text{ads},\infty} + 4\sigma V_M/d$ . From this positive change in adsorption free energy, the adsorption equilibrium constant follows:<sup>58</sup>

$$K_{\text{ads}}(d) = K_{\text{ads},\infty} \exp\left(-\frac{4\sigma V_M}{dRT}\right) \quad (3)$$

where  $R$  is the gas constant,  $T$  is temperature, and  $K_{\text{ads},\infty}$  is the adsorption equilibrium constant to the bulk material surface. Equation 3 predicts that the adsorption equilibrium constant will decrease with decreasing size of the nanoparticle, as observed for  $K_1$  (Table 1 and Figure 5A).

The size effect on adsorption kinetics is derived through the Brønsted–Polanyi relation  $k = gK^\alpha$ , where  $k$  is the rate constant,  $K$  is the equilibrium constant,  $g$  is a proportionality constant, and  $\alpha$  is the Brønsted–Polanyi parameter and  $0 < \alpha < 1$ .<sup>24,59–61</sup> Following eq 3, the adsorption and desorption rate constants of a molecule to a nanoparticle are:<sup>58</sup>

$$k_{\text{ads}}(d) = gK_{\text{ads}}(d)^{\alpha_{\text{ads}}} = k_{\text{ads},\infty} \exp\left(-\frac{4\alpha_{\text{ads}}\sigma V_M}{dRT}\right) \quad (4)$$

$$k_{\text{des}}(d) = k_{\text{des},\infty} \exp\left(\frac{4(1 - \alpha_{\text{ads}})\sigma V_M}{dRT}\right) \quad (5)$$

where  $k_{\text{ads},\infty}$  and  $k_{\text{des},\infty}$  are the adsorption and desorption rate constants to the bulk surface, and  $\alpha_{\text{ads}}$  is the Brønsted–Polanyi parameter for the adsorption rate constant. If the catalysis follows the Langmuir–Hinshelwood mechanism, the rate constant for the catalytic conversion reaction after reactant adsorption is given by Murzin:<sup>58</sup>

$$k_{\text{cat}}(d) = k_{\text{cat},\infty} \exp\left(\frac{4(1 - \alpha_{\text{cat}})\sigma V_M}{dRT}\right) \quad (6)$$

$\alpha_{\text{cat}}$  here is the Brønsted–Polanyi parameter for the rate constant of the catalytic conversion reaction. Equation 6 predicts that with decreasing particle size,  $k_{\text{cat}}(d)$  will increase, as observed for the catalytic conversion of resazurin to resorufin by the Au-nanoparticles ( $\gamma_{\text{eff}}/A$ , Table 1 and Figure 5B).

To fit the size dependence of  $K_1$  and  $\gamma_{\text{eff}}/A$  with eqs 3 and 6, we further included the size dependence of the surface tension,  $\sigma$ , from thermodynamic analysis:<sup>62–64</sup>

$$\sigma(d) = \sigma_\infty \left(1 - \frac{1}{(2d/h) - 1}\right) \exp\left(-\frac{2S_b}{3R} \frac{1}{(2d/h) - 1}\right) \quad (7)$$

Here,  $\sigma_\infty$  is the surface tension of the bulk material,  $h$  is the atomic diameter,  $S_b (=E_b/T_b)$  is the cohesive entropy of the bulk material,  $E_b$  is the bulk cohesive energy, and  $T_b$  is the bulk solid–vapor transition temperature.

The above thermodynamic model fits the size dependence of  $K_1$  and  $\gamma_{\text{eff}}/A$  satisfactorily (Figure 5A,B); the fitted corresponding values for bulk gold surfaces are  $600 \pm 50 \mu\text{M}^{-1}$  and  $(0.18 \pm 0.03) \times 10^{-3} \text{ s}^{-1} \text{ nm}^{-2}$ , respectively (Table 1). The Brønsted–Polanyi parameter  $\alpha_{\text{cat}}$  for  $\gamma_{\text{eff}}/A$  is  $0.23 \pm 0.05$ , smaller than 0.5, suggesting an early transition state for the catalytic conversion of resazurin to resorufin.

**Product Dissociation Reaction.** For the product dissociation reaction, the two product dissociation rate constants,  $k_2$  and  $k_3$ , both decrease with decreasing particle size, suggesting a strengthened adsorption of the product resorufin on the Au-nanoparticle surface as compared to that to the bulk gold surface. Therefore, the adsorption of resorufin to the Au-nanoparticles corresponds to the case that the change in adsorption free energy from the nanosize effect is negative, that is,  $\Delta G_{\text{ads}}(d) = \Delta G_{\text{ads},\infty} - 4\sigma V_M/d$ . Using the Brønsted–Polanyi relation, similarly as described earlier, the size effect on the rate constant of desorption (i.e., dissociation) follows:<sup>57</sup>

$$k_{\text{des}}(d) = k_{\text{des},\infty} \exp\left(-\frac{4\alpha_{\text{ads}}\sigma V_M}{dRT}\right) \quad (8)$$

Here,  $\alpha_{\text{ads}}$  is the Brønsted–Polanyi parameter for the corresponding adsorption rate constant. Equation 8 predicts that with decreasing particle size, the rate constant of desorption will decrease, as observed for  $k_2$  and  $k_3$  (Table 1 and Figure 5C,D). Combining eqs 7 and 8 to fit the results in Figure 5C and D gives the corresponding values of  $k_2$  and  $k_3$  on bulk gold surfaces and the associated  $\alpha_{\text{ads}}$ 's (Table 1).

The opposite changes in adsorption free energy from the nanosize effect for the substrate resazurin and for the product resorufin suggest their different bonding interactions with the Au-nanoparticle surface. One possibility is that in the adsorbate–surface bonding, the gold atom(s) on the nanoparticle surface effectively acts as electron acceptor for interacting with resazurin, whereas for interacting with resorufin, it acts as electron donor. With decreasing particle size, both the unoccupied and the occupied electronic states of the Au-nanoparticles increase in energy, weakening the acceptor interactions with resazurin while strengthening the donor interactions with resorufin. Future studies using quantum mechanical calculations may provide more understanding into the bonding interactions of resazurin and resorufin with Au-nanoparticle surfaces.<sup>19,61</sup>

**4.2. Kinetics and Energetics of Dynamic Surface Restructuring.** The single-particle turnover trajectories reveal temporal activity fluctuations in both the  $\tau_{\text{off}}$  reaction (i.e., catalytic product formation) and the  $\tau_{\text{on}}$  reaction (i.e., product dissociation), which are attributable to catalysis-induced and spontaneous dynamic surface restructuring (section 3.3). The time scales of the underlying dynamic surface restructuring are obtainable from the autocorrelation functions of  $\tau_{\text{off}}$  and  $\tau_{\text{on}}$  and show strong dependence on both the rate of turnovers and the nanoparticle size (Figure 4). The rates of the activity fluctuations (and thus the underlying dynamic surface restructuring) increase linearly with increasing rates of turnovers, reflecting the catalysis-induced contributions. The extrapolations of activity fluctuation rates to zero rate of turnovers approximate the rates of spontaneous dynamic surface restructuring (Figure 4C,D), which

(59) Bronsted, J. N. *Chem. Rev.* **1928**, *5*, 231.

(60) Evans, M. G.; Polanyi, M. *Trans. Faraday Soc.* **1938**, *34*, 11.

(61) *Chemical Bonding at Surfaces and Interfaces*; Nilsson, A., Pettersson, L. G. M., Norskov, J. K., Eds.; Elsevier: Amsterdam, 2008.

(62) Jiang, Q.; Li, J. C.; Chi, B. Q. *Chem. Phys. Lett.* **2002**, *366*, 551.

(63) Lu, H. M.; Jiang, Q. *J. Phys. Chem. B* **2004**, *108*, 5617.

(64) Yang, C. C.; Li, S. *Phys. Rev. B* **2007**, *75*, 165413.

(65) Tyson, W. R. *Surf. Sci.* **1977**, *62*, 267.

(66) Slater, J. C. *J. Chem. Phys.* **1964**, *41*, 3199.

(67) Nanda, K. K. *Appl. Phys. Lett.* **2005**, *87*, 021909.

(68) Kittel, C. *Introduction to Solid State Physics*, 5th ed.; Wiley: New York, 1976.

(69) *CRC Handbook of Chemistry and Physics*, 76th ed.; Lide, D. R., Ed.; CRC Press, Inc.: Boca Raton, FL, 1995.

become faster with decreasing size, consistent with the less stable surfaces of smaller nanoparticles. In this section, we formulate a simple model to analyze quantitatively the catalysis- and size-dependent dynamic surface restructuring of Au-nanoparticles.

On the basis of the experimental observations (Figure 4C,D), we can approximate a linear relation between  $r$ , the rate of dynamic surface restructuring of a Au-nanoparticle, and  $v$ , its rate of turnovers:

$$r = r_{\text{sp}} + pv \quad (9)$$

where  $r_{\text{sp}}$  is the rate of spontaneous dynamic surface restructuring and  $p$  is a parameter that couples the catalysis to surface restructuring. Because how readily catalysis can induce surface restructuring should be correlated with how readily spontaneous surface restructuring can occur, we can approximate that the coupling parameter  $p$  is linearly proportional to  $r_{\text{sp}}$  as  $p = qr_{\text{sp}}$ , and  $q$  here is a proportionality constant. This approximation is reasonable, as the ratios between the intercepts and the slopes of the linear fits in Figure 4C and D do not vary significantly across the different-sized Au-nanoparticles (Table S2). We then have:

$$r = r_{\text{sp}} + qr_{\text{sp}}v = r_{\text{sp}}(1 + qv) \quad (10)$$

The rate of spontaneous dynamic surface restructuring,  $r_{\text{sp}}$ , can be related to its activation energy  $\Delta E_{\text{sp}}$ :

$$r_{\text{sp}} = r_{\text{sp}}^0 \exp(-\Delta E_{\text{sp}}/RT) \quad (11)$$

where  $r_{\text{sp}}^0$  is the rate of spontaneous dynamic surface restructuring when thermal energy is much larger than the activation energy. As surface restructuring involves breaking or partial breaking of the bonding between particle surface atoms,  $\Delta E_{\text{sp}}$  should be proportional to the atom–atom bond strength and thus to the cohesive energy  $E(d)$  of the nanoparticle; therefore, we can write:

$$\Delta E_{\text{sp}} = \beta E(d) \quad (12)$$

where  $\beta$  is a proportionality constant. The cohesive energy  $E(d)$  is dependent on the particle size and follows a relation with the particle diameter similar to that of the surface tension in eq 7.<sup>62–64</sup>

$$E(d) = E_{\text{b}} \left( 1 - \frac{1}{(2dl/h) - 1} \right) \exp \left( -\frac{2S_{\text{b}}}{3R} \frac{1}{(2dl/h) - 1} \right) \quad (13)$$

where  $E_{\text{b}}$  is the bulk cohesive energy.

Combining eqs 10–13, we can fit the catalysis- and size-dependent dynamic surface restructuring in Figure 4C and D satisfactorily (Figure 6A,B). The fits give  $\beta = 0.061 \pm 0.006$ ,  $r_{\text{sp}}^0 = 20 \pm 18 \text{ s}^{-1}$ ,  $q_{\tau_{\text{off}}} = 21 \pm 9 \text{ s}$ , and  $q_{\tau_{\text{on}}} = 43 \pm 17 \text{ s}$ . The different values of  $q$  for the  $\tau_{\text{off}}$  and  $\tau_{\text{on}}$  reactions come from the different coupling strengths between the reactions and the surface restructuring, with the  $\tau_{\text{on}}$  reaction more effective in inducing surface restructuring, as reflected by the larger slopes in Figure 4D than those in Figure 4C.

The  $\tau_{\text{on}}$  reaction being more effective than the  $\tau_{\text{off}}$  reaction in inducing surface restructuring is consistent with their associated changes in surface–adsorbate interactions. The larger the net change is in adsorbate–surface interactions, the greater surface restructuring it will cause. The  $\tau_{\text{off}}$  reaction includes the fast adsorption–desorption equilibrium of the substrate resazurin and the catalytic conversion of resazurin to resorufin. The perturbations on the surface by fast adsorption and fast desorption are opposite in effect and thus cancel each other. The net

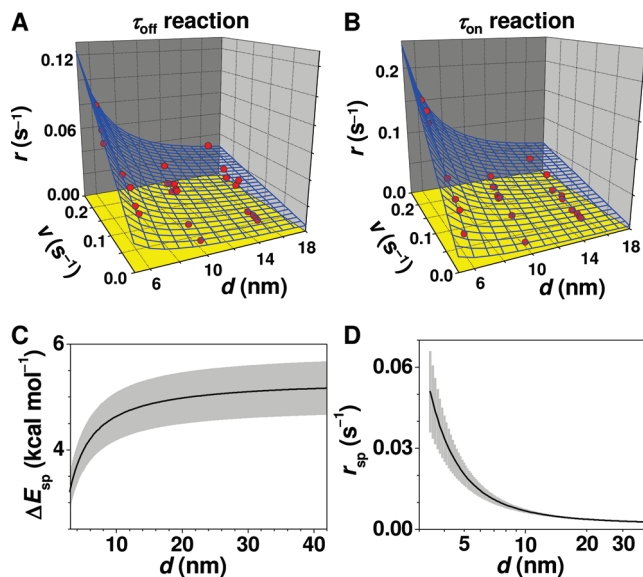


**Figure 6.** (A,B) Surface restructuring rate ( $r$ ) dependence on the rate of turnovers ( $v$ ) and the nanoparticle diameter ( $d$ ). Fitting parameters:  $\beta = 0.061 \pm 0.006$ ,  $r_{\text{sp}}^0 = 20 \pm 18 \text{ s}^{-1}$ ,  $q_{\tau_{\text{off}}} = 21 \pm 9 \text{ s}$ , and  $q_{\tau_{\text{on}}} = 43 \pm 17 \text{ s}$ . (C,D) Size dependence of the activation energy ( $\Delta E_{\text{sp}}$ ) and the rate ( $r_{\text{sp}}$ ) of the spontaneous dynamic surface restructuring of Au-nanoparticles. The gray shades denote the approximate errors from the error bars of  $\beta$  and  $r_{\text{sp}}^0$ .

change of adsorbate–surface interaction in  $\tau_{\text{off}}$  reaction is thus the difference between resazurin–surface and resorufin–surface interactions. On the other hand, the  $\tau_{\text{on}}$  reaction is the product dissociation reaction. The net change of adsorbate–surface interaction here is the loss of resorufin–surface interaction, which is greater than the difference between the resazurin–surface and the resorufin–surface interactions. Therefore,  $\tau_{\text{on}}$  reaction would result in greater net changes in adsorbate–surface interaction and thus be more effective in inducing surface restructuring.

Using the fitted value of  $\beta$ , we can obtain the estimates of  $\Delta E_{\text{sp}}$ , the activation energy of spontaneous dynamic surface restructuring, across different sizes of Au-nanoparticles (Figure 6C). In the range of 6–15 nm diameters,  $\Delta E_{\text{sp}}$  is  $\sim 4.5 \text{ kcal mol}^{-1}$ , and it increases to  $>5 \text{ kcal mol}^{-1}$  for bulk gold surfaces, which is comparable to the activation energy ( $\sim 12 \text{ kcal mol}^{-1}$ ) measured for reconstruction of bulk Au surfaces.<sup>70</sup> As compared to the bulk cohesive energy  $E_{\text{b}}$  ( $\sim 87 \text{ kcal mol}^{-1}$ ) of gold,<sup>67,68</sup> the small magnitude of  $\Delta E_{\text{sp}}$  suggests that this surface restructuring does not require complete breaking of surface atom bonding interactions and likely involves only partial breaking of surface atom bonding; concerted rearrangements of surface atoms are also possible, in which partial breaking and formation of surface atom bonding occur simultaneously.

The estimated spontaneous surface restructuring rate  $r_{\text{sp}}$  is  $\sim 0.004\text{--}0.017 \text{ s}^{-1}$  in the range of 6–15 nm, corresponding to a time scale of 60–250 s, and it slows asymptotically to  $\sim 0.003 \text{ s}^{-1}$  for bulk gold surfaces (Figure 6D). Although the model used here is simple and does not consider factors such as solvent effects and possible changes in surface chemical nature during catalysis, the values of  $\Delta E_{\text{sp}}$  and  $r_{\text{sp}}$  here provide direct estimates of the energetics and structural dynamics of metal surface atoms

(70) Pierce, M. S.; Chang, K.-C.; Hennessy, D. C.; Komanicky, V.; Menzel, A.; You, H. *J. Phys. Chem. C* **2008**, *112*, 2231.

in an aqueous environment, which are fundamentally important for heterogeneous catalysis in all size scales.

## 5. Summary

Using single-molecule microscopy of fluorogenic reactions, we have studied the catalytic activity and dynamics of individual spherical Au-nanoparticles of three different sizes under ambient solution conditions. By monitoring the catalysis of individual nanoparticles in real time with single-turnover resolution, we observe clear size-dependent activities in both the catalytic product formation reaction and the product dissociation reaction. With decreasing particle size, the substrate binding affinity decreases, concurrent with an increase in reactivity of catalytic conversion per surface area. In contrast, the product binding affinity increases with decreasing particle size, reflected by a decrease of the rate constants in the two product dissociation pathways. Within a model of classical thermodynamics, these size-dependent activities can be accounted for by the changes in the adsorption free energies of the substrate resazurin and the product resorufin that result from the nanosize effect of the Au-nanoparticles.

Besides affecting catalytic activity, size also affects the differential selectivity of the Au-nanoparticles between the two parallel product dissociation pathways. Larger nanoparticles are less selective between the two pathways. This size-dependent selectivity is particularly challenging to quantify in ensemble-averaged measurements, but is readily approachable with single-particle measurements.

The particle size also strongly influences the surface-restructuring-coupled catalytic dynamics; both the catalysis-induced and the spontaneous dynamic surface restructuring occur more readily for smaller Au-nanoparticles due to their higher surface energies. Assuming a linear coupling between catalysis and surface restructuring and using the size dependence of the cohesive energy of nanoparticles, we analyze the catalysis- and size-dependent dynamic surface restructuring quantitatively. The results provide estimates on the activation energies and time scales of spontaneous dynamic surface restructuring that are fundamental to heterogeneous catalysis in both the nano- and the macro-scale. The results from our study exemplify the power of single-molecule approach in probing the intricate workings of nanoscale catalysts.

**Acknowledgment.** We thank the Army Research Office (56355-CH), the National Science Foundation (CBET-0851257), the NSF-funded Cornell Center for Materials Research, the Petroleum Research Foundation (47918-G5), Alfred P. Sloan Research Fellowship, and the Camille and Henry Dreyfus Foundation New Faculty Award for financial support, and J. S. Kong for help with TEM measurements.

**Supporting Information Available:** Experimental scheme, additional results, and analyses. This material is available free of charge via the Internet at <http://pubs.acs.org>.

JA904307N